International Journal of Precision Engineering and Manufacturing
https://doi.org/10.1007/s12541-024-00990-0

Online ISSN 2005-4602
Print ISSN 2234-7593

REGULAR PAPER

Design and Control of a Flexure-Based Dual Stage Piezoelectric Micropositioner

Romina Zarrabi Ekbatani[1] · Jinchuan Zheng[1] · Xiaoqi Chen[2] · Mostafa Nikzad[3] · Zhihong Man[1]

Received: 5 December 2023 / Revised: 3 March 2024 / Accepted: 5 March 2024

Abstract
In the field of advanced manufacturing technology, there is a growing need for high-precision micro/nano positioners. The traditional single stage actuated positioners have encountered performance limitation in achieving longer travel range and higher precision. This motivates us to develop a novel dual stage piezoelectric-actuated micropositioner presented in this paper. The micropositioner incorporates displacement amplification mechanisms to overcome the limited range of piezoelectric actuators. Design considerations such as flexure characteristics and material selection are discussed, and structural analysis is performed using finite element analysis (FEA). For precise positioning, the dual stage control strategy is investigated and compared with the conventional proportional-integral-derivative (PID) single stage control method. In the proposed positioner, a combination of parallelogram and bridge mechanisms is utilized. The bridge mechanism works to amplify the piezoelectric actuator displacement output. The parallelogram mechanism, integrated within the system, helps mitigate resonance modes and contributes to the achievement of linearized motion. The characteristics of the micropositioner were evaluated using analytical modelling and FEA. Multiple analysis was used to optimise the positioner's design parameters. Furthermore, experimental studies were carried out to validate the characteristics of the micropositioner performance in terms of achievable output travel range and sustained positioning accuracy.

Keywords Piezoelectric actuator · Parallelogram mechanism · Bridge-type mechanism · Dual stage control · Micropositioner

1 Introduction

Piezoelectrically actuated micropositioning systems have emerged as a significant technological breakthrough, finding extensive use in various fields, notably in scanning probe microscopy and nanometrology [1–4]. These systems are celebrated for their precision and the capability to operate at high frequencies, reaching hundred hertz. The use of piezoelectric tube scanners, which were previously widespread in scanning probe microscopy [5, 6], has seen a decline as piezoelectric stack-actuated stages have become more prevalent. This shift is attributed to their enhanced range of motion, superior mechanical bandwidth, and reduced cross-coupling effects among different axes.

Piezoelectric substances are considered as a type of functional ceramics that have the ability to transform electrical energy into mechanical energy [7–11]. These materials possess various advantages such as prompt response, high precision, compactness, and stiffness, making them a perfect actuation source for precision positioning systems. [12–15]. Nonetheless, their output displacement is usually restricted to less than 0.1% of their longitudinal length, thereby constraining their usage [16, 17]. It is necessary to make use of the amplification mechanisms in order to get around this problem. More specific, the lever mechanism, the bridge mechanism, and the Scott-Russell (SR) mechanism are three common examples of displacement amplification mechanisms [18].

✉ Romina Zarrabi Ekbatani
rominazarrabi@swin.edu.au

[1] School of Science, Computing and Engineering Technologies, Swinburne University of Technology, John St, Hawthorn 3122, VIC, Australia

[2] Shien-Ming Wu School of Intelligent Engineering, South China University of Technology, Guangzhou International Campus, Wushan Rd, Guangzhou, China

[3] School of Engineering, Swinburne University of Technology, John St, Hawthorn 3122, VIC, Australia

Published online: 27 March 2024

The lever mechanism is an example of a displacement-amplification mechanism that is both straightforward and efficient [19, 20]. Xing and colleagues, in their study [21], developed a gripper by integrating a single-lever mechanism with a flexible parallel four-bar mechanism, resulting in a ratio of displacement amplification being 4.16. Nonetheless, the amplification capability of a solitary lever usually does not exceed a factor of 10. Thus, the utilization of a compound lever magnifying mechanism could be considered for extended magnification.

Various lever mechanisms with deformable structures, such as levered parallelograms and right-angle levers, are in use. The right-angle lever, specifically designed for perpendicular motion conversion, usually features input and output ends at right angles to each other [22–24]. This design has been effectively employed by researchers like Wang et al. in creating grippers for precise manipulation tasks [24]. Notable for its simplicity, robustness, energy conservation, and linear amplification characteristics, the L-shaped lever mechanism, however, faces limitations in amplification due to spatial constraints. Additionally, based on the mechanical advantage, increasing the output arm's displacement inversely affects the clamping force.

The Scott-Russell (SR) mechanism is designed to transform orthogonal displacement into linear output in response to a specific input displacement. By connecting multiple SR mechanisms in series, it's possible to enhance the magnification ratio. Studies on the SR mechanism indicate that the orientation and positioning of the flexure hinge play crucial roles in determining both magnification and linearity ratios. Often, the SR mechanism is employed alongside other amplification mechanisms to meet particular objectives. For example, combining it with lever or parallelogram mechanisms has led to the development of grippers with unique functionalities. An advanced version of the SR mechanism has demonstrated a 3.56-fold increase in magnification ratio over traditional designs. Additionally, the SR mechanism has found applications in guiding micromanipulators and as an integral part of microgrippers, known for their high natural frequencies. The bridge mechanism, widely recognized in the field of amplification mechanisms [19, 25], operates on the compression linkage instability principle from materials mechanics. This principle suggests that when an input force is applied, the flexible hinge in the mechanism deforms to produce movement in a direction orthogonal to the input. Bridge mechanisms often employ right-angle or round flexural joints to facilitate substantial motion amplification. Although offering more compact designs for equivalent amplification compared to lever mechanisms, bridge mechanisms present more intricate displacement analysis models [26]. Researchers such as Lobontiu, Ma, Qi, Ye, and Lin have advanced various models of the bridge mechanism, each based on distinct principles of kinematics and mechanics [27, 28].

To achieve single-sided or double-sided output, piezoelectric is commonly embedded in the centre of the bridge mechanism [29, 30]. Piezoelectric materials are often integrated into the center of bridge mechanisms for generating either single-sided or double-sided output. In systems where piezoelectric elements are used for actuation, bridge mechanisms that are aligned longitudinally typically produce a double-sided output. Liang and colleagues strategically placed both the bridge mechanism and the piezoelectric element at the center of their clamp design, mitigating the effects of shearing stress and bending moment on the actuator. Conversely, bridge mechanisms aligned horizontally are more inclined to yield a single-sided output [31–33]. Furthermore, to extend the clamping stroke, bridge structures can be arranged either in series or parallel. The series configuration of bridge mechanisms uses a limited space to attain a higher amplification ratio [34], exemplified by Chen et al.'s approach of linking two bridge mechanisms in series to enhance the stroke of the end-effector. Parallel arrangements typically feature a common fixed end [35, 36]. Xu's design of a flexible composite bridge mechanism stands out for its high magnification ratio, compactness, and robust lateral stiffness [29, 30].

The bridge-type mechanism has benefits such as high rigidity, load-bearing capacity, and a large working range, which make it suitable for a wide range of applications. On the other hand, the Scott-Russell and lever-type mechanisms have some disadvantages. They have a limited range of motion, nonlinear output, and lower rigidity and stability compared to the bridge-type mechanism. Additionally, the Scott-Russell and lever-type mechanisms have lower load-bearing capacity, which can restrict their use in applications that require high force or weight handling. Despite these disadvantages, these mechanisms can still be useful in specific applications where their limitations are not a significant concern. Hence, in this paper the combination of flexures and bridge-type mechanism has been used for designing the micropositioner.

Table 1 A comparison of key characteristics of flexure-based mechanisms

Literature	Amplification ratio	Accuracy (μm)	Travel range (μm)
Xing et al. [21]	4.2	7.5	249.4
Zhang et al. [37]	6.0	0.6	60
Zhang et al. [38]	22.8	N/A	190
Wang et al. [39]	18.1	N/A	310.2
Our proposed design	28.17	1	648

In summary, Table 1 offers a detailed comparison of key characteristics of flexure-based mechanisms as documented in existing research. Previous studies, including those by Xing et al. [21] with an amplification ratio of 4.2, Zhang et al. [37] achieving 6.0, another study by Zhang et al. [38] at 22.8, and Wang et al. [39] reporting 18.1, have contributed valuable insights into this field. Remarkably, our proposed design surpasses these figures with an amplification ratio of 28.17, alongside superior accuracy at 1 μm and an extensive travel range of 648 μm, marking a significant advancement over the documented works.

In piezoelectric-actuated mechanisms, advanced control methodologies are utilized to achieve precise positioning, high performance, and real-time motion. Currently, proportional-integral-derivative (PID) control is a commonly utilized approach due to its effectiveness and independence from models. Carrozza et al. utilized a proportional-integral (PI) strategy to attain precise and consistent grip force control in the assembly of microelectromechanical systems [40].

Nevertheless, the PID controller is frequently unable to fulfil the requirements because micropositioning often involves the presence of high-frequency dynamic force vibration. This limitation led to the development of the sliding mode control (SMC), which performs better than the PID force controller in terms of force regulation performance. To address this, Wang et al. devised a novel position/force switching control scheme by combining an incremental PID controller and discrete SMC [41]. Based on the experimental results, the proposed strategy demonstrated high-speed, accurate, and robust micro-operation. In a similar case, Liang et al. incorporated different specific control strategies in their position/force switching control scheme. In this instance, the gripper's motion position was regulated using a PID controller, favored for its straightforward feedback loop and easily adjustable parameters [42]. Additionally, Wu and associates recommended an adaptive backstepping SMC approach to counteract hysteresis effects [43]. Sliding mode control can suffer from high-frequency chattering, sensitivity to uncertainties and modeling errors, and difficulties in design and implementation [18, 44]. To overcome the disadvantages by existing methods, the dual stage control method was proposed by using two actuating control loops that combine a high-gain feedback controller to provide robustness against uncertainties and a low-gain feedback controller to smooth out the control signal and improve positioning accuracy. As a result, the dual stage control has been shown to provide better disturbance rejection, reduced chattering, and improved stability in certain applications compared to SMC approaches [45].

The concept of a dual-stage system, characterized by the integration of coarse and fine stages for achieving long stroke, rapid, and accurate placement, has been introduced as an advancement over traditional single-stage positioners. In such systems, the coarse stage is employed for broader and larger motion range, while the fine stage is dedicated to more precise and smaller range adjustments. Typically, the fine stage has minimal force and limited displacement, but enhanced accuracy, while the coarse stage has the opposite characteristics. By adopting the benefits of both coarse and fine stages, it is possible to create a motion control system with a large workspace and high resolution. Numerous studies have utilised the concept of dual stage compound stages. Several works, for instance, are available on macro/micro manipulators. Presently, the most dynamic research in dual stage servo systems is being conducted in the area of hard disc drives (HDD) [46–48], where fine actuators made through micromachining technology facilitate rapid track following. This study employs two types of piezoelectric actuators - one designed for long-range and the other for short-range movements - as an alternative to a voice coil motor (VCM), aiming to enhance accuracy and leverage the advantages of piezoelectric actuators.

1.1 Objectives and Outlines

The primary objectives of this study are as follows:

- Design a dual stage micropositioner combined with novel flexure-based displacement amplification systems and a high-bandwidth platform to simultaneously achieve a large displacement range and high precision in a small form factor.
- Develop the dual stage micropositioner prototype with appropriate dual stage controller to achieve the desired positioning performance.
- Conduct experiments on the fabricated prototype to verify the performance of the design and development.

The design of micropositioner is described in Sect. 2. This is followed by a discussion on a variety of design factors, including flexure characteristics, the material employed, rigidity and piezoelectric actuator rigidity. ANSYS is used to do the FEA analysis on modal shape and static analysis. Section 3 describes the experimental setup and system identification for the two stages on the micropositioner and simulation results are given. The dual stage controller is described in Sect. 4, where the performance of single stage and dual stage control methods is also compared.

2 Design of the Dual Stage Micropositioner

The proposed dual stage micropositioner is designed based on the principles of flexible mechanisms, specifically utilizing a combination of a parallelogram mechanism and a bridge-type mechanism [49, 50]. These flexure-based

mechanisms rely on the elastic deformation of the structures to generate precise motion. This design approach offers several advantages, including the ability to generate substantial forces and achieve high accelerations, which are crucial for developing a high-bandwidth positioning stage. In the following, the design and prototyping of the micropositioner will be thoroughly described to provide detailed insights into the development process.

2.1 Design Description

To amplify the displacement of piezo actuators, most piezo-actuated positioners incorporate flexure-based mechanical amplification mechanisms. Because a piezoelectric stack actuator can only produce displacement of about 0.1% of the piezo stack's length [51, 52], movement is limited to several tens of micrometres. As a result, mechanical amplification mechanisms are essential for applications requiring tens to hundreds of microns. To achieve precise motion, the micropositioner incorporates a bridge-type mechanism as well as parallelogram mechanisms. The embedded piezoelectric actuator produces an output displacement that drives the mechanism's input ends. The bridge-type mechanism then amplifies the resultant movement to increase the total displacement of the system.

The parallelogram linkages are critical in ensuring the linear motion of the output of the micropositioner. They effectively reduce any unwanted cross-directional translational displacement of the stage. The micropositioner has a compact design thanks to the use of a single stage amplification mechanism. This design is made possible by the use of right-angle flexural hinges, which allow the mechanism to form revolute joints. In certain applications, the right-angle flexural hinge is preferred over circular hinges due to its ability to evenly distribute stress and provide lower resistance to movement at the mechanism's input point. This makes it a more suitable option when there is a need for the hinge to withstand forces without causing stress concentration in one specific area, as well as when flexibility and responsiveness to external forces are desired. This enables the mechanism to be driven effectively with small piezoelectric actuators [53].

The proposed dual stage micropositioner is composed of two parts:

- The first stage, which contains flexure-based amplification mechanisms to supply a large displacement output.
- The second stage, which contains flexure-based mechanisms of a high stiffness to ensure the high precision at the dual stage position output.

The required input displacement is provided by two piezoelectric stack actuators, one for each stage. A bridge-type and parallelogram mechanism with right-angle flexure hinges was employed to achieve a high amplification ratio in the first stage. The parallelogram mechanism is frequently utilized in conjunction with displacement amplification mechanisms to achieve parallel motion. This combination allows for the generation of synchronized and coordinated motion across multiple elements or stages in a system [54]. By incorporating the parallelogram mechanism in a serial configuration with the displacement amplification mechanism, the system can effectively produce parallel motion, enabling precise and coordinated movement in various applications. Among various mechanisms, the bridge-type mechanism is considered for amplification purposes in this paper. Figure 1a shows such a mechanism, which consists of twelve parallel elements arranged in a bridge configuration. When a voltage is applied to the piezoelectric actuator, it creates a displacement perpendicular to the applied force. The main advantage of this mechanism type lies in its ability to facilitate movement in both directions. This means that it can provide both pushing and pulling forces, which is essential for accurate and stable positioning. Additionally, the bridge-type mechanism provides a larger displacement range compared to other mechanisms, which is important for achieving high precision and accuracy. Furthermore, the bridge-type mechanism has a high stiffness and low hysteresis, which ensures precise and repeatable positioning. The low hysteresis also allows for fast response time, making it suitable for high-speed applications. Figure 1b shows the design for the secondary stage, aimed at offsetting the inaccuracies introduced by the first stage, and thus it is designed with a mechanism of high stiffness and without displacement amplification. Figure 1c shows the final assembled mechanisms, leading to the dual stage micropositioner.

One of the main objectives in the design of the first stage was to enhance the amplification ratio of the mechanism by decreasing the flexure hinges thickness. Through experimentation and analysis, it was determined that the minimum manufacturable thickness for the design was 0.3 mm, which resulted in an amplification ratio of 28.17. This represents a notable advancement over the previous amplification ratio reported in the literature. The findings were obtained by utilizing wire electric discharge machining (WEDM) techniques and materials. Figure 2 depicts the displacement of the stage, which shows that the maximum output displacement is increased from 310 μm to 648 μm when the beam thickness decreases from 0.8 mm to 0.3 mm.

As seen in Fig. 1, the proposed mechanism consists of two stages, where the first stage is equipped with a piezoelectric stack that enables long-range motion within 674 μm range. The second stage is attached to the first stage and moves in tandem without any amplification ratio, operating within

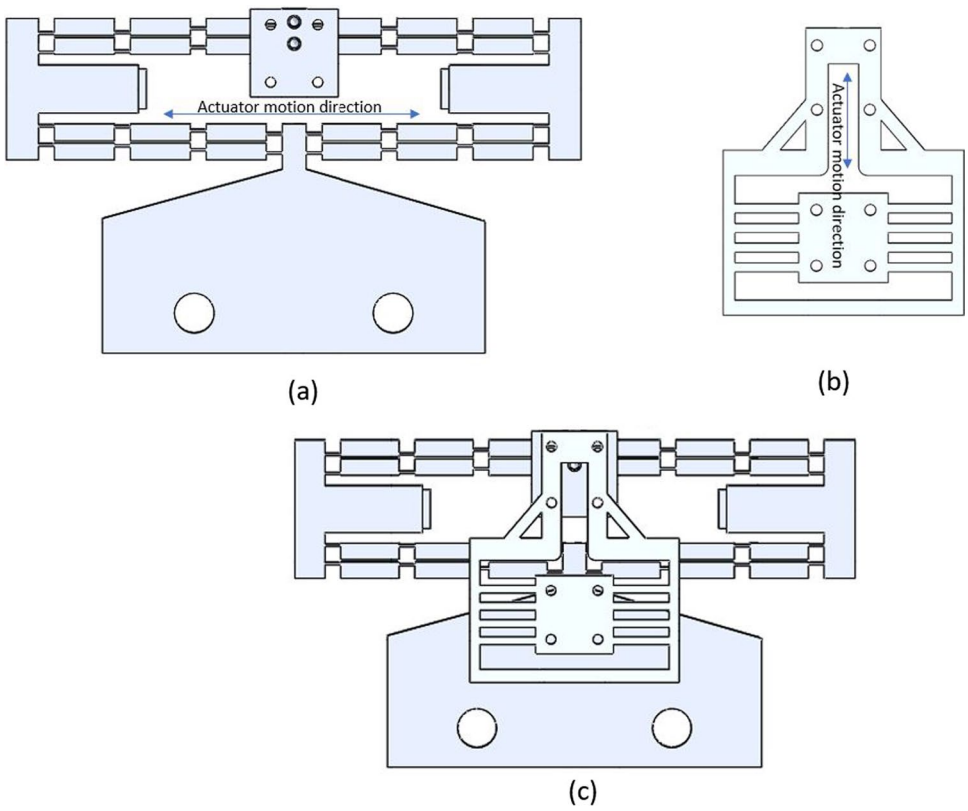

Fig. 1 **a** First stage design by using parallelogram bridge-type mechanism **b** Second stage design **c** Assembled dual stage mechanism

a range of 12 μm. A total of 24 beam flexures are implemented for the stages, chosen for their increased flexibility and capacity to provide larger motion ranges compared to circular flexures. This design effectively addresses the need for precise and controlled motion within a specific range, while also ensuring optimal functionality and reliability.

The pseudo-rigid-body model (PRBM) is extensively used in the examination and development of compliant mechanisms. In this model, the flexural hinges of the mechanism are represented as simplified right-angle flexures [53]. Based on the quasi-rigid-body approximation and PRBM methodology, these simplified right-angle flexures are equivalent to the combination of two fixed linkages, a pivot joint and a rotational spring [55]. Figure 3 depicts this modeling procedure.

Additionally, considerations such as the displacement of centres of rotation and the rigidity of orthogonal flexural hinges are overlooked. Figure 4 showcases the PRBM (Parallel Right-Angle Bridge Mechanism) of the initial design stage under review. In this figure, $A - H$ and $A' - H'$ denote the centers of rotation of the compact orthogonal elastic joints, Δ_{in} represents the movement at the input point, and Δ_{out} indicates the resulting movement of the micropositioner.

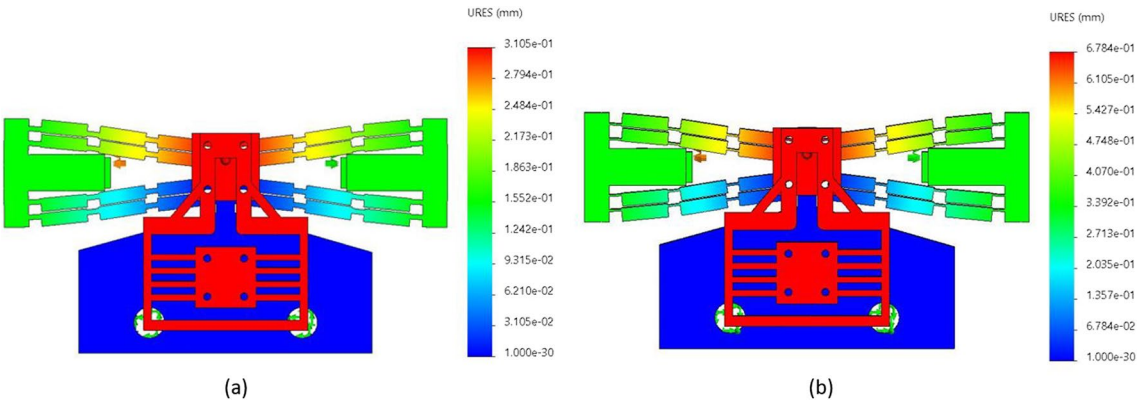

Fig. 2 **a** Maximum displacement with 0.8 thickness **b** Maximum displacement with 0.3 thickness

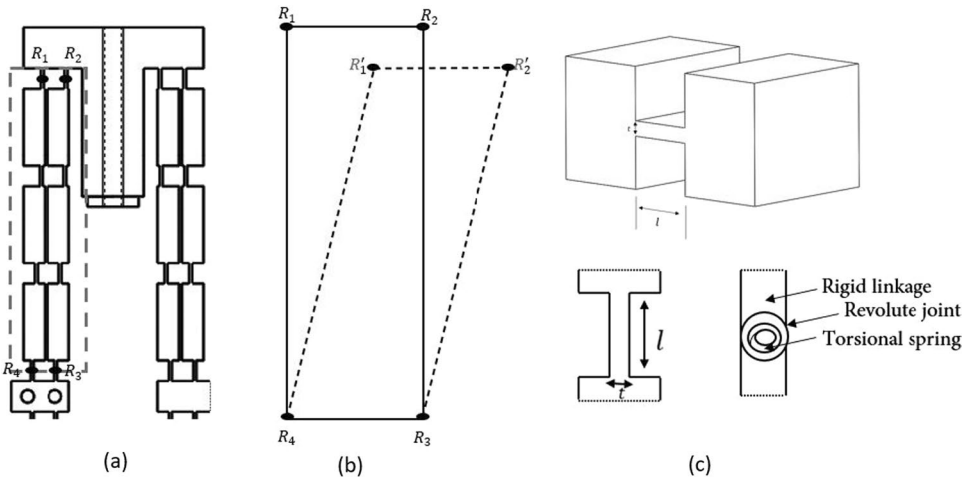

Fig. 3 **a** Parallelogram mechanism used in the first stage **b** PRBM of the mechanism prior to and following displacement **c** A compact orthogonal flexure and its PRBM

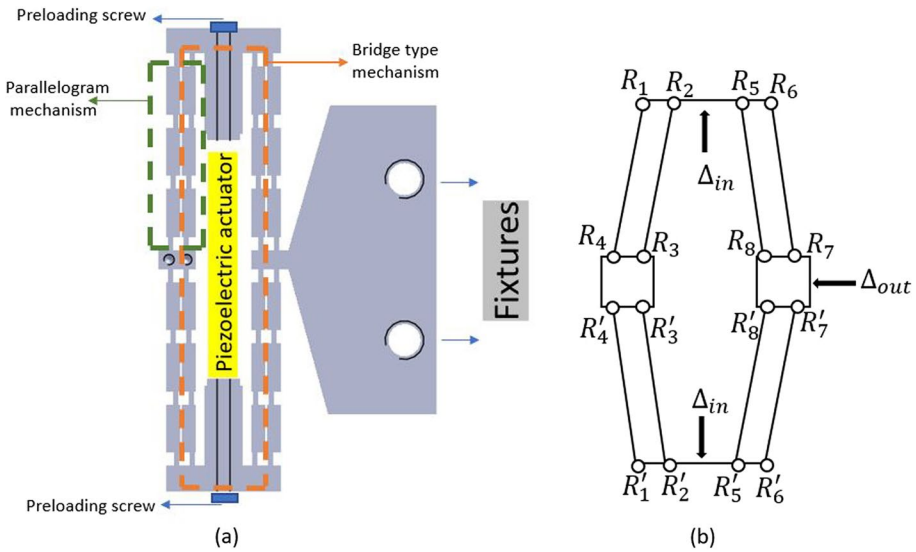

Fig. 4 First stage design of the micropositioner **a** CAD drawing **b** PRBM representation

Analyzing the design of the amplification system reveals a bridge-type mechanism represented by a four-bar linkage $R_1 - R_2 - R_3 - R_4$, which can be incorporated on one side of the structure, as illustrated in Fig. 5. In this arrangement, θ_1, θ_2, θ_3, and θ_4 correspond to the initial angles of the linkages R_1R_2, R_2R_3, R_3R_4, and R_4R_1 respectively. The direction of tangential velocity for the link R_1R_2 at point R_2 is represented by β. The geometric specifications of the micropositioner are detailed in Table 2. All right-angle flexures within the micropositioner maintain a consistent length, denoted as l, and a planar thickness, indicated by t. The thickness of these flexures is 0.3 mm.

The examination of the dynamic interrelation between geometric and kinematic properties in the $R_1 - R_2 - R_3 - R_4$ four-bar linkage system validates its effectiveness in precisely depicting linkage relationships, as adapted from Das (2020) [53, 56]:

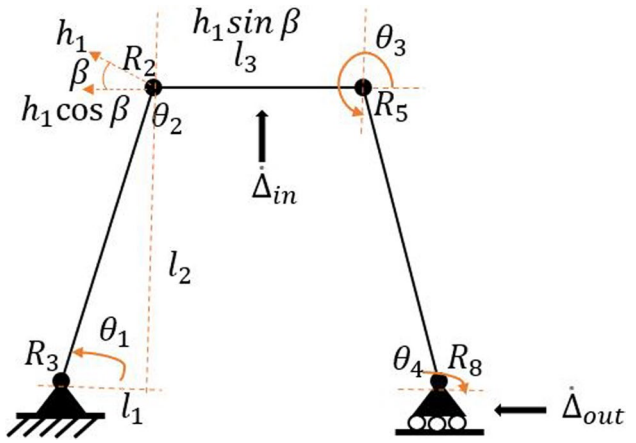

Fig. 5 Bridge-type mechanism

Table 2 Principal design parameters of the micropositioner

Parameters	l	t	l_1	l_2	l_3
Values (mm)	2	0.3	2.7	30.5	14.3

$$l_{R_1R_4}e^{i\theta_4} = l_{R_1R_2}e^{i\theta_1} + l_{R_2R_3}e^{i\theta_2} + l_{R_3R_4}e^{i\theta_3} \tag{1}$$

Application of Euler's formula facilitates the derivation of x and y displacement components:

$$l_{R_1R_4}\cos\theta_4 = l_{R_1R_2}\cos\theta_1 + l_{R_2R_3}\cos\theta_2 + l_{R_3R_4}\cos\theta_3 \tag{2}$$

$$l_{R_1R_4}\sin\theta_4 = l_{R_1R_2}\sin\theta_1 + l_{R_2R_3}\sin\theta_2 + l_{R_3R_4}\sin\theta_3 \tag{3}$$

Further differentiation of Eqs. (2) and (3) yields:

$$\dot{\Delta}out\sin\theta 4 = l_{R_1R_2}\omega_1\sin\theta_1 + l_{R_2R_3}\omega_2\sin\theta_2 + l_{R_3R_4}\omega_3\sin\theta_3 \tag{4}$$

$$\dot{\Delta}out\cos\theta 4 = l_{R_1R_2}\omega_1\cos\theta_1 + l_{R_2R_3}\omega_2\cos\theta_2 + l_{R_3R_4}\omega_3\cos\theta_3 \tag{5}$$

Under specific angular conditions ($\theta_2 = 0$, $\theta_4 = 2\pi$, $\omega_2 = \omega_3$), the following is obtained:

$$\dot{\Delta}out = lR_1R_2\omega_1\sin\theta_1 + l_{R_3R_4}\omega_3\sin\theta_3 \tag{6}$$

$$l_{R_1R_2}\omega_1\cos\theta_1 + \omega_3(l_{R_2R_3} + l_{R_3R_4}\cos\theta_3) = 0 \tag{7}$$

Substitution of ω_3 from (7) into (6) leads to:

$$\dot{\Delta}out = lR_1R_2\omega_1\left(\sin\theta_1 - \frac{\sin\theta_3\cos\theta_3 l_{R_3R_4}}{l_{R_2R_3} + l_{R_3R_4}\cos\theta_3}\right) \tag{8}$$

Tangential velocity at R_2 is described by:

$$v_1 = \omega_1 l_{R_1R_4} \tag{9}$$

$$v_1 = \frac{\dot{\Delta}in}{2\sin\beta} \tag{10}$$

Substitution of β=π-θ1 and v_1 into (8) results in the amplification ratio:

$$r_{amp} = \frac{\dot{\Delta}out}{\dot{\Delta}in} = -\frac{1}{2\cos\theta_1}\left(\cos\theta_1 + \frac{\sin\theta_3\cos\theta_3 l_{R_3R_4}}{l_{R_2R_3} + l_{R_3R_4}\cos\theta_3}\right) \tag{11}$$

This design focuses on developing a compact micropositioner with an enhanced amplification ratio, structured to facilitate integration with a secondary stage for ultra-precise manipulation. Prior literature [56, 57] underscores the necessity for a high resonance frequency, which in turn dictates a design with both compactness and rigidity. As a result, the dimensions of the flexures are minimized, which naturally elevates the stage's resonance frequency while curtailing its range of motion. To strike an equilibrium between these elements, iterative design processes were conducted using ANSYS software, ensuring adherence to predefined design requirements, with key parameters presented in Table 2. The flexures' thicknesses were meticulously calibrated to extend the travel range and bolster the stage's resonance frequency.

Material choice is pivotal, as the stage's resonance frequencies are influenced by the material properties. Opting for a material characterized by both high Young's modulus of elasticity E and low density ratio ρ enhances the stage's mechanical rigidity and operational bandwidth. An aluminium alloy 7075-SN (Al 7075), known for its high modulus-to-density ratio with $E = 72$ GPa and $\rho = 2.81$ g/cm^3, was selected for construction.

The system's design process included an in-depth assessment of the stage's structural stiffness K_s, which is integral to the performance of the coupled piezoelectric stack actuator. This examination is crucial to define the piezoelectric stack actuator's maximum displacement, which is governed by K_s, depicted by the equation:

$$\Delta L = \frac{K_{Piezo}}{K_s + K_{Piezo}}\Delta L_0 \tag{12}$$

Here, ΔL_0 signifies the piezoelectric stack actuator's maximum displacement without external spring load, ΔL represents the displacement when subjected to an external spring load, K_s indicates the stage's structural rigidity, and K_{Piezo} quantifies the piezoelectric stack actuator's stiffness. Elevating K_s is imperative for enhancing the stage's resonance frequencies, yet it inversely affects the maximum displacement ΔL. To reconcile these factors, K_s is set to be roughly 10% lower than K_{Piezo}, fostering a harmonious balance. The selected piezoelectric stack actuator, with a robust K_{Piezo} of 50 N/m, ensures a substantial K_s and elevates the mechanical resonance frequency without significantly diminishing the motion span. Ultimately, the positioner is designed to reach a primary resonance frequency of 88 Hz and a motion extent of 674 μm.

2.2 Prototyping and Analysis

Figure 6 presents the prototype of the proposed micropositioner fabricated by using WEDM. The piezoelectric actuators (PI P−885.91 for the first stage and P−883.31 for the second stage) are also mounted in the micropositioning

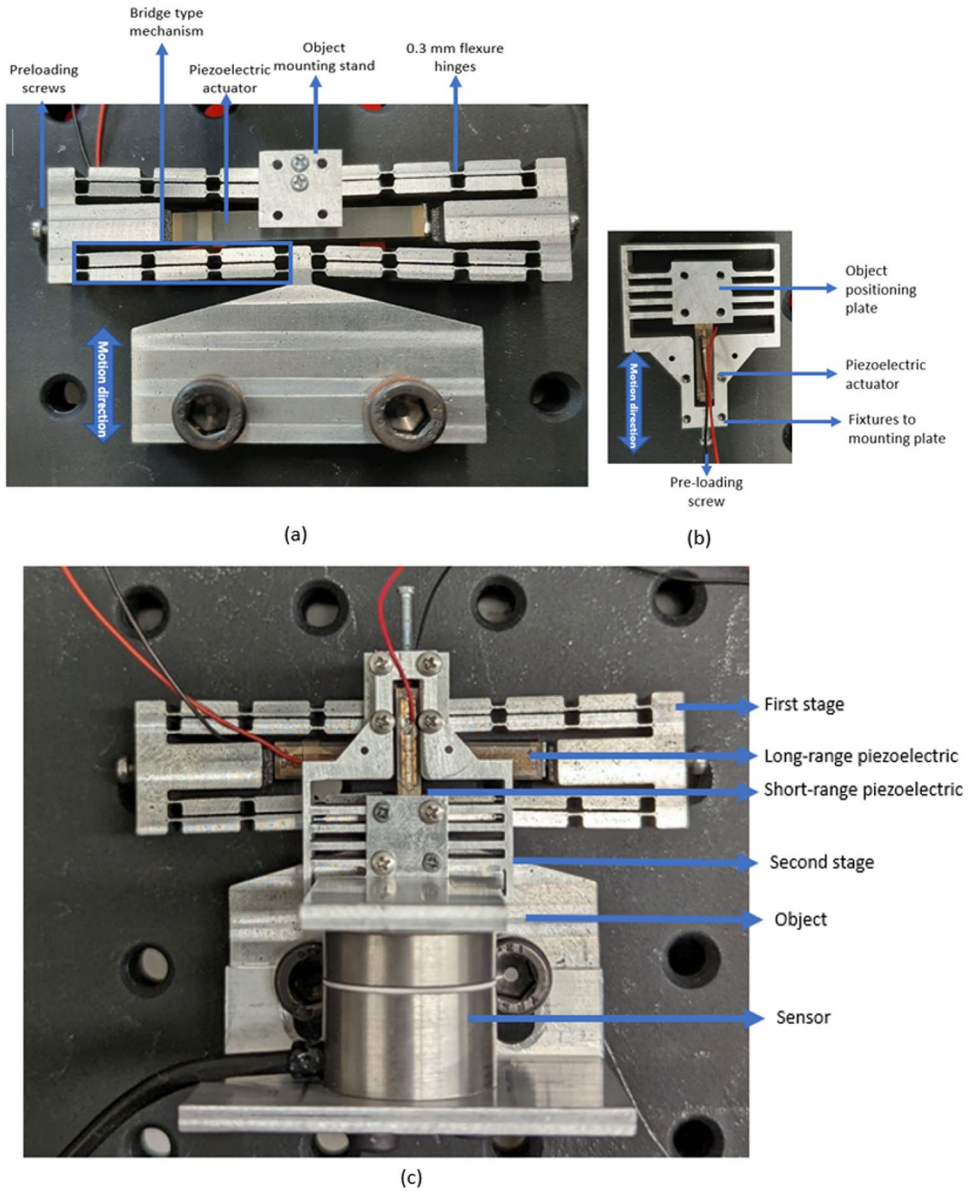

Fig. 6 Fabricated prototype of the micropositioner. **a** First stage **b** Second stage **c** Assembled dual stage

mechanism. The stage is fixed on top of a steel plate of 10 mm thickness to maintain its position securely. The second stage consists of four sets of threaded holes for attaching it to the mounting plate as well as four other mounting holes for the fixtures that sit between the first and second stages. As illustrated in Fig. 6, a small aluminum surface block, featuring a smooth surface finish, is attached to the platform stage. This block acts as the target for a capacitive displacement sensor (MicroSense 8810), which is used to measure the stage's output displacement. In addition, a real-time control system (dSPACE-DS1103) is utilized to implement the controller for the piezoelectric actuators. The sampling rate for the real-time controller in the study is established at 1 kHz.

2.2.1 Stress Analysis

This section investigates the stress distribution characteristics of the assembled micropositioner, as illustrated in Fig. 7.

In the Finite Element Method (FEM) analysis of the dual-stage micropositioning system, a highly detailed mesh size was employed to accurately model the intricate features of the mechanism. For the simulation, the second stage of the micropositioner was modeled as a load on the first stage, applied as a force. The force along with the displacement, was applied at both ends of the piezoelectric elements, representing the actual operational conditions. The material selected for the FEM analysis is aluminium 7075-SN, consistent with the material used in

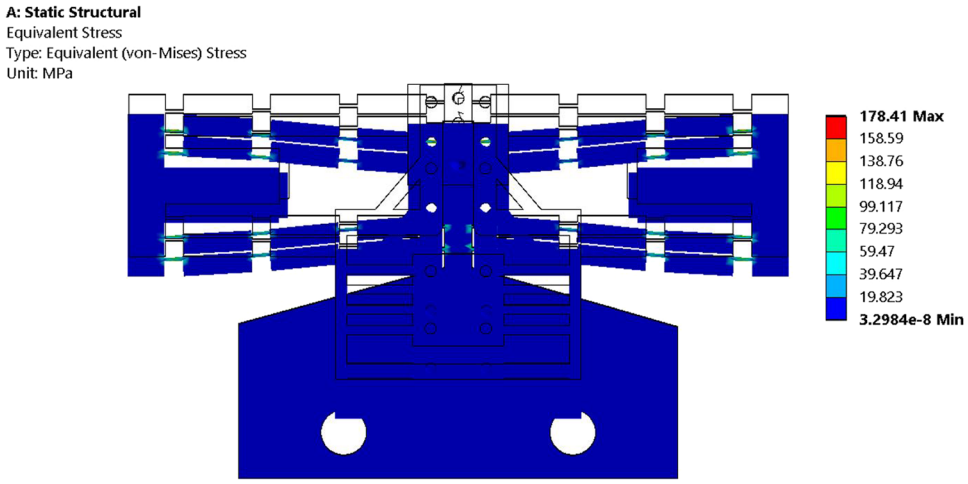

Fig. 7 Stress analysis results

the fabrication of the actual positioning stage. This choice ensures that the simulation closely mirrors the physical properties and responses of the real-world system. The maximum stress is 148.42 Mpa appearing at the flexure connected with the fixed part of the mechanism. The information obtained from this analysis can serve as a valuable reference for optimizing the performance of the micropositioner and improving its overall structural reliability for future mechanism design.

2.2.2 Modal Shape Analysis

The modal shape frequencies for each constituent stage, specifically the first and second stages, must be examined in the context of the dual stage configuration. These modal shape frequencies are critical indicators of their dynamic behaviours.

The modal frequencies in the first stage, depicted in Fig. 8a–c, are as follows: the first mode shape resonates at 117 Hz, while the second and third mode shapes resonate at 171 Hz and 416 Hz, respectively. The modal frequencies correspond to the first, second, and third mode shapes of the second stage, are shown in Fig. 9a–c. The first modal shape registers at 729 Hz, the second mode shape at 1530 Hz, and the third mode shape at 2160 Hz at this stage. These frequencies represent the vibrational characteristics of the second stage of the dual stage configuration.

Furthermore, the modal characteristics of the assembled dual stage system have improved, resulting in a wider frequency range. Figure 10a shows the first modal shape, which is 80 Hz. Moving on to the second modal shape, it has a frequency of 161 Hz, as shown in Fig. 10b. Finally, as shown in Fig. 10c, the third modal shape has a frequency of 241 Hz.

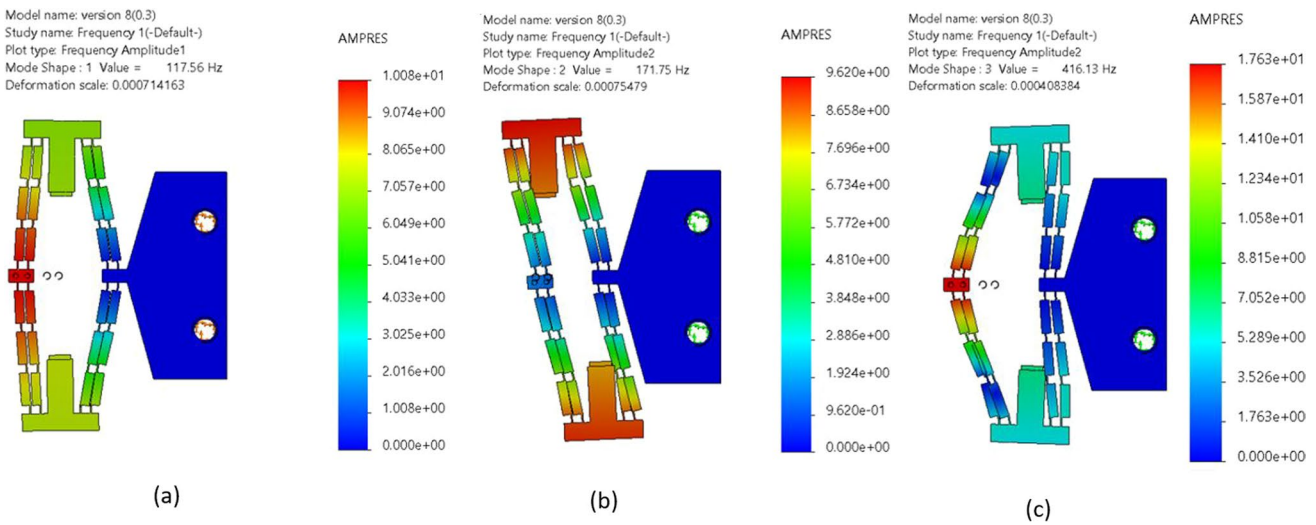

Fig. 8 First stage modal shapes. **a** First mode **b** Second mode **c** Third mode

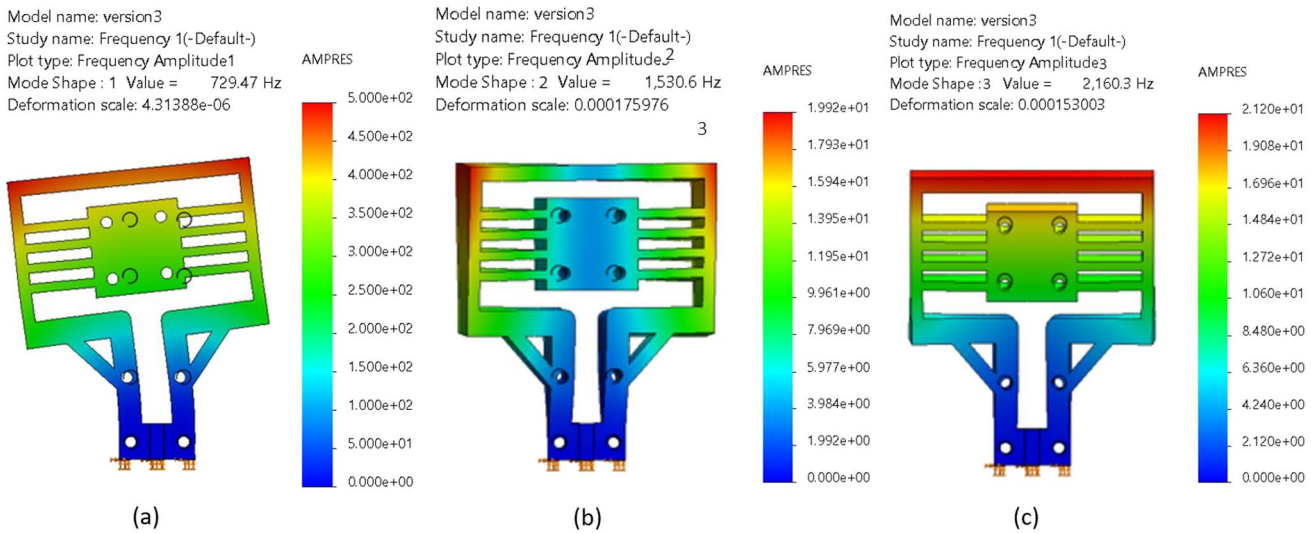

Fig. 9 Second stage modal shapes. **a** First mode **b** Second mode **c** Third mode

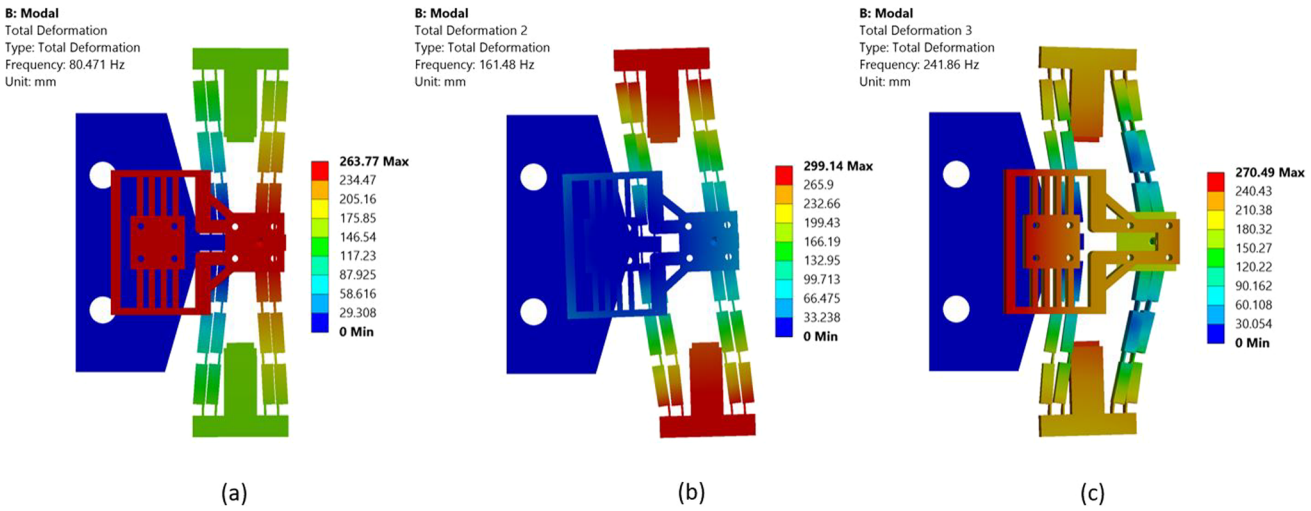

Fig. 10 Modal shape analysis of the dual stage micropositioner. **a** First mode **b** Second mode **c** Third mode

3 System Identification and Verification

3.1 Identified Model

In this section, the mathematical models for the first and second stage are respectively identified by using the measured model data and frequency-domain identification method.

3.1.1 First Stage Model

The model data is measured by using a dynamic signal analyzer (DSA), This creates the swept-sinusoidal stimulation signals and gathers data on the frequency response resulting from the output of these excitation signals. After that, based on the measured frequency response data, discrete Fourier transform (DFT) in MATLAB's invert frequency approach was used to identify the transfer function of the stage. Without solving the whole differential equation, the transfer function offers a framework for determining crucial system response characteristics.

After examining the order of the transfer function, and using the Invfreqs, it was found that 16 zeros and 17 poles provided the best fit for both the modal shape and the phase plot. Figure 11 depicts Bode diagram of both ithe identified

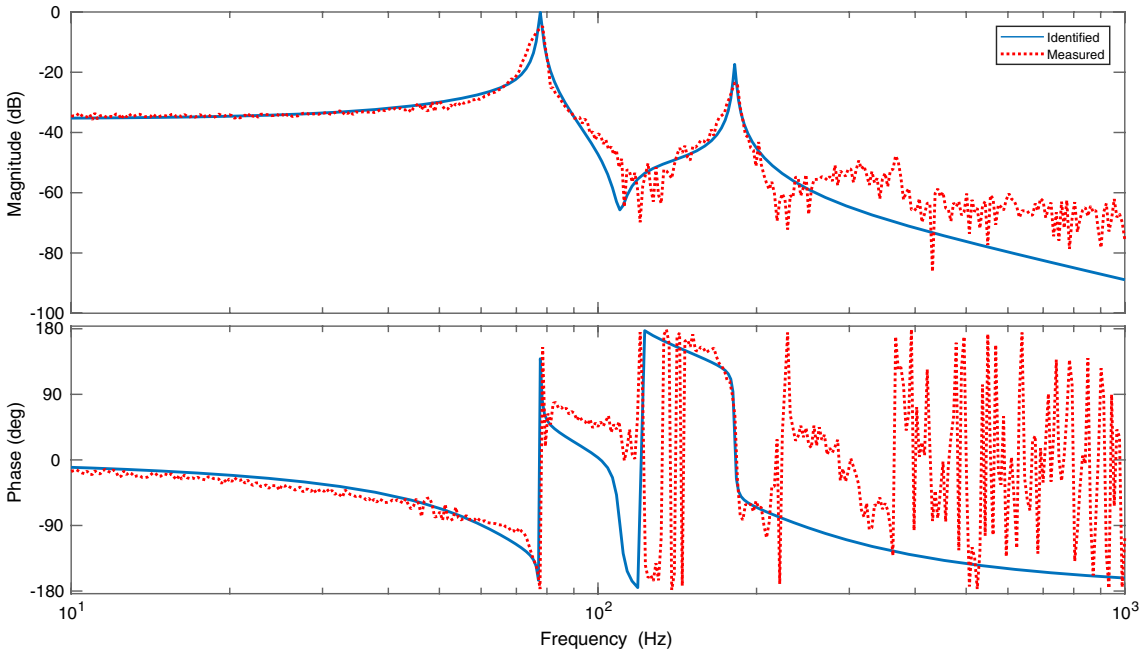

Fig. 11 System model of the first stage under dual-stage assembly

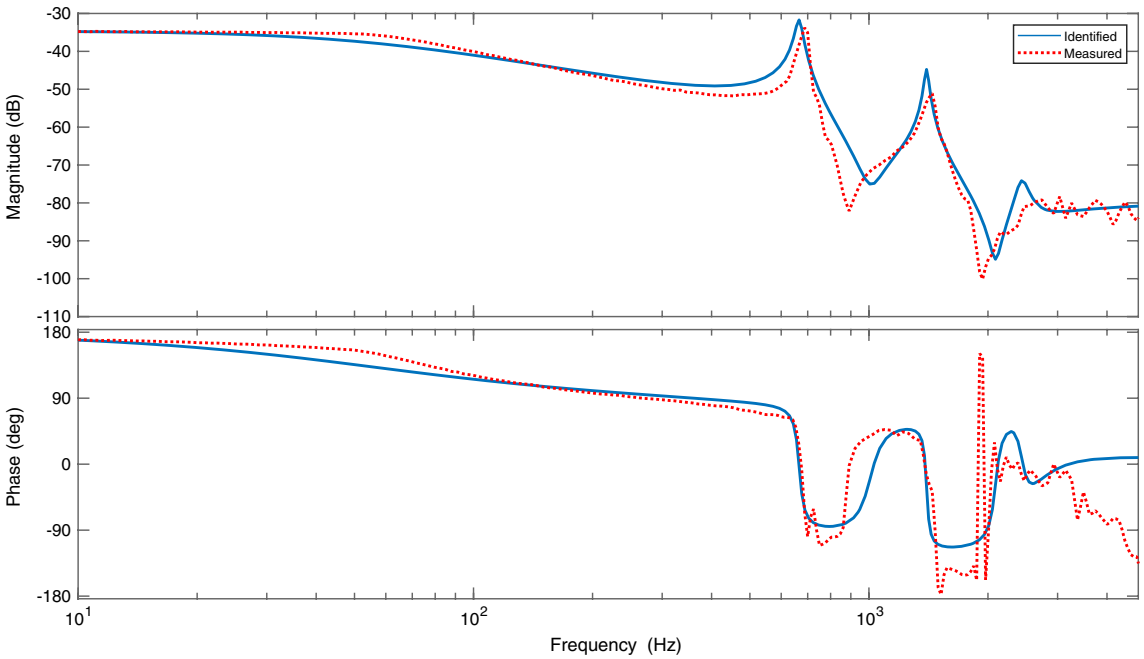

Fig. 12 System model of the second stage under dual-stage assembly

model and measured model. Since the order of this model is high and developing a PID controller for such a model is difficult, a model reduction algorithm was used to remove the high-frequency portion of the model. The model order was reduced from 17 to 6 by weighting the fit-errors versus frequency. As such, the final transfer function model for the first stage mechanism can be expressed as follows:

$$P_1(s) = \frac{(s^2 - 1.5154s + 1.5711)(s^2 - 0.0256s + 0.4769)}{(0.001465s^2 + 1.145118s + 1.14248)(s^2 + 0.184008s + 0.17353)} \tag{13}$$

3.1.2 Second Stage Model

Following the same procedure as conducted on the first stage modeling, the modeling results for the second stage mechanism are shown in Fig. 12.

The identified transfer function for the second stage consists of 8 poles and 4 zeros with the following expression:

$$P_2(s) = \frac{(s^2 - 3.5464s + 3.9837)(s^2 + 0.4733s + 6.3519)}{(s^2 - 0.146s + 5.9442)(s^2 + 0.0472s + 2.1599)(s^2 + 0.0125s + 2.0069)(s + 0.0535)} \tag{14}$$

4 Control Design

Dual stage positioning systems are commonly used in many applications, particularly in the fields of optics and semiconductor manufacturing, where precise positioning is essential. In a dual stage system, two actuators are used to independently control the motion of two cascaded stages, enabling high precision along a large working range. The two-stage system allows for high bandwidth and dynamic range, which are particularly useful in applications that require fast and accurate motion control. Additionally, dual stage systems have a high load capacity, making them ideal for use in applications where a large payload needs to be moved with high precision.

Another advantage of dual stage positioning systems is their versatility. By using two independent actuators, dual stage systems can achieve both large and small movements with high precision, making them ideal for a wide range of applications. Moreover, dual stage systems can be designed to provide precise control over both linear and rotational movements, making them an attractive option for use in applications that require both types of motion. Additionally, dual stage systems can be combined with other control systems, such as optical encoders or strain gauges, to achieve even greater levels of precision and control. Overall, the high precision, versatility, and load capacity of dual stage positioning systems make them an excellent choice for a wide range of applications in which precise positioning is critical.

4.1 Decoupled Master–Slave Control Structure

This paper employs the decoupled master–slave control structure to design the controller for the developed dual stage positioner. The control structure is shown in Fig. 13, which consists of a master loop (the second stage loop denoted by P_2C_2) and a slave loop (the first stage denoted by P_1C_1) to collaboratively achieve fast and accurate positioning control. The slave loop (i.e., the first stage) will carry out the primary control action in response to the reference and disturbance input, which may result in a coarse positioning precision. On the other hand, the master loop (i.e, the second stage) has a faster and finer dynamic performance and will ensure to compensate for the residual tracking error caused the slave loop. In

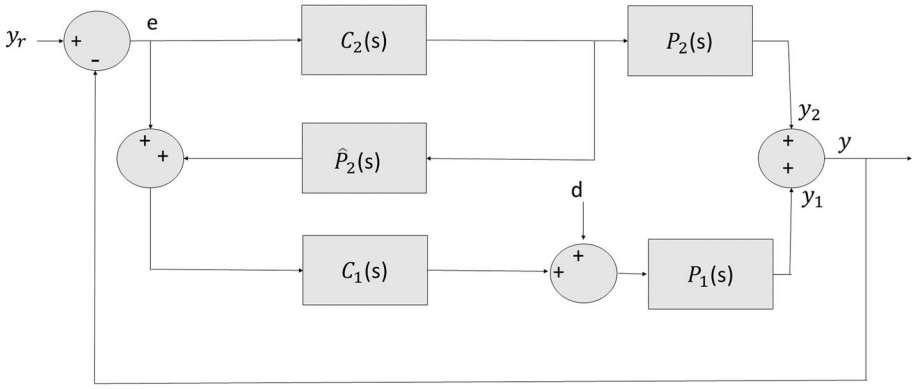

Fig. 13 Decoupled master–slave control structure for the dual stage positioner

addition, the expression $\hat{P}_2(s)$ denotes the estimated model of the second stage, and it is set as equivalent to $P_2(s)$ to decouple the behaviour between the master and slave loop.

In the development of the dual-stage micropositioner, a Proportional-Integral-Derivative (PID) controller was selected over Sliding Mode Control (SMC) due to its simplicity and effectiveness in our specific application. This decision was driven by the nature of the system, which did not exhibit significant uncertainties or disturbances that typically necessitate the robustness of SMC. The PID controller, with its straightforward feedback mechanism, adequately met the system's requirements, allowing for reliable trajectory tracking while maintaining the focus on the mechanical design and development of the stage. To analyze the stability of dual stage control system, denote $G_1 = P_1C_1$ and $G_2 = P_2C_2$ and assume $\hat{P}_2(s) = P_2(s)$. Hence, the closed-loop transfer function of the system can be easily obtained by

$$H_{cl} = \frac{y}{y_r} = \frac{G_1 + G_2 + G_1G_2}{(1 + G_1)(1 + G_2)}. \tag{15}$$

Obviously, for a given set of controllers C_1 and C_2, the dual stage control system is stable if all the poles of (15) are in the left half-plane.

In addition, the disturbance rejection transfer function in response to the disturbance input at P_1 as shown in Fig. 13 is given by:

$$H_d = \frac{y}{d} = \frac{P_1}{(1 + G_1)(1 + G_2)}. \tag{16}$$

Equation (16) indicates that a smaller value of $H_d(s)$ will result in better disturbance rejection performance. By adding the second stage, it is clear that $H_d(s)$ has a further reduction of gain by the ratio of $(1 + G_2)$. This validates the principle of dual stage control system in enhancing the tracking accuracy.

The following equations show the final designed dual-stage controllers, both of which are cascaded PI-controller with a notch filter to compensate for the first resonance mode in each stage:

$$C_1 = \left(0.0006 + \frac{250}{s}\right)\left(\frac{s^2 + 0.004\pi 90s + \pi 180^2}{s^2 + 0.9\pi 90s + \pi 180^2}\right) \tag{17}$$

$$C_2 = \left(0.0001 + \frac{400}{s}\right)\left(\frac{s^2 + 0.009\pi 1000s + \pi 2000^2}{s^2 + 0.07\pi 1000s + \pi 2000^2}\right) \tag{18}$$

4.2 Experimental Results

The purpose of this study was to improve the performance of a single stage positioner by using the dual stage approach. Firstly, the single stage positioner was tested under a 3 μm

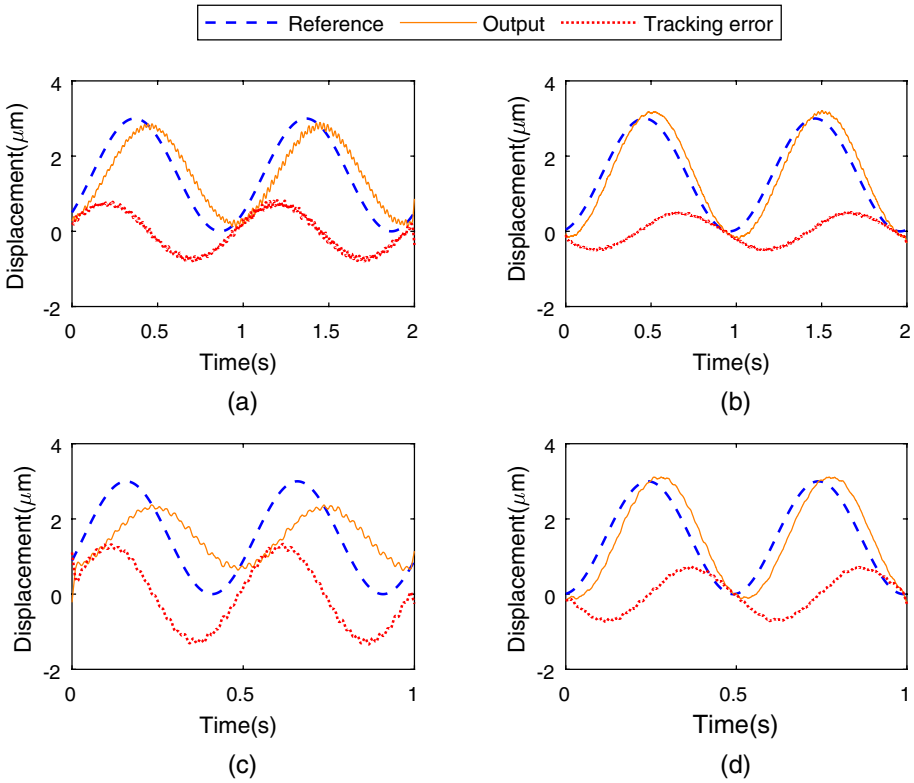

Fig. 14 Tracking performance comparison. **a** Single stage under a 3 μm and 1 Hz sine wave reference, **b** Dual stage with 3 μm and 1 Hz sine wave reference, **c** Single stage with 3μm and 2 Hz sine wave reference, **d** Dual stage with 3 μm and 2 Hz sine wave reference

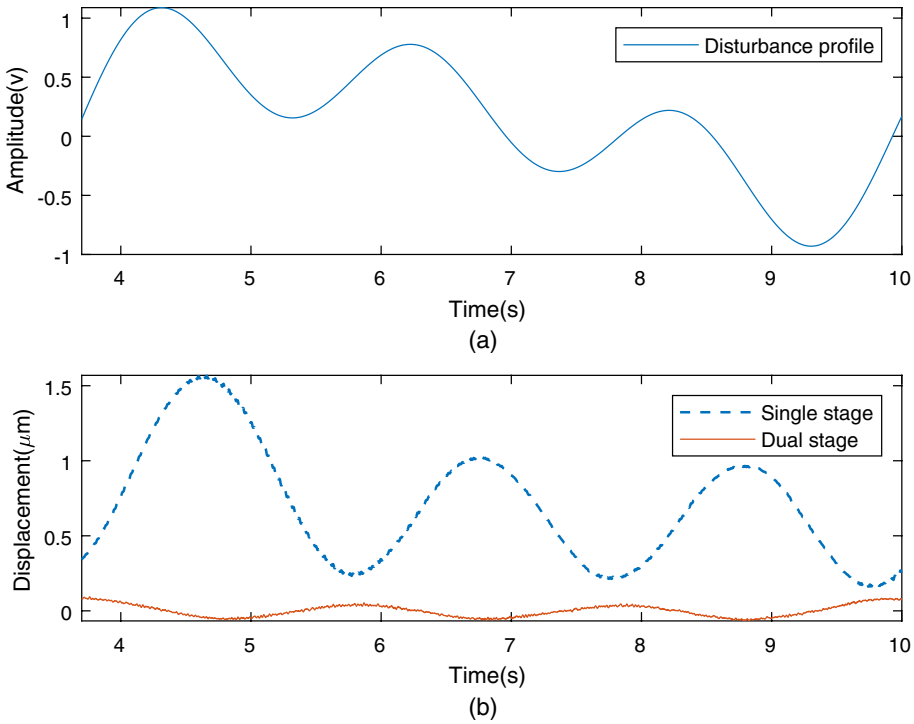

Fig. 15 Disturbance rejection. **a** Disturbance profile, **b** Position output

sine wave reference at both 1 Hz and 2 Hz, while the dual stage positioner was also tested under the same reference profiles. Figure 14 show that the dual stage positioner outperforms the single stage one in terms of tracking error reduction. Specifically, when the frequency is 1 Hz, the improvement on the tracking error was 43%. The mean absolute value for the single stage under 1-Hz sine wave reference was 0.5691, while for the dual stage it was 0.3225. Similarly, for 2-Hz sine wave reference, the improvement was 46%, with 0.8470 for the single stage and 0.4512 for the dual stage experiments. These results suggest that the addition of a second stage to the system is highly beneficial in terms of improving tracking accuracy. This can be attributed to the fact that the second stage significantly compensates for the errors introduced by the first stage, leading to a more accurate dual stage system.

Secondly, disturbance rejection experiments were conducted to further evaluate the performance of the systems as shown in Fig. 15. The results showed a significant improvement by the dual stage positioner, with the mean absolute value of 0.0408, compared to 0.7129 for the single stage system. This indicates that the dual stage system is highly effective in rejecting the disturbances, further highlighting its superior performance. The results of this study suggest that a dual stage system is more effective than a single stage system in terms of accuracy and disturbance rejection. These findings have important implications for the design and implementation of precision control systems in various applications. The first stage, while precise due to its PZT actuator, is designed primarily for a large displacement amplification, resulting in lower stiffness and a slower response speed. This design optimizes the working range. The second stage, by contrast, focuses on enhancing response speed and accuracy. Control gain tuning was meticulously optimized, considering the trade-off between response speed and tracking accuracy, particularly in the context of amplified sensor noise at higher gains. This dual-stage design strategy effectively addresses the inherent limitations of PZT stages in terms of working range and dynamic performance.

Third, experiments were carried out to assess the tracking performance when using a staircase reference. The purpose of these experiments was to compare the settling time and tracking error of the single stage control with that of the dual stage control. The results obtained from the experiments indicate notable difference between the two control configurations as shown in Fig. 16. In addition, Fig. 17 shows the tracking errors profiles that corresponding to the period from 8.5 to 14 s in Fig. 16 for a clearer comparison. It can be seen that for the single stage control, the settling time was found to be approximately 0.7 s. In contrast, the dual stage control exhibited a significantly improved settling time of 0.2 s, representing a remarkable 71% reduction in settling time. This outcome demonstrates the advantage of utilizing a dual stage control system in terms of achieving faster response time.

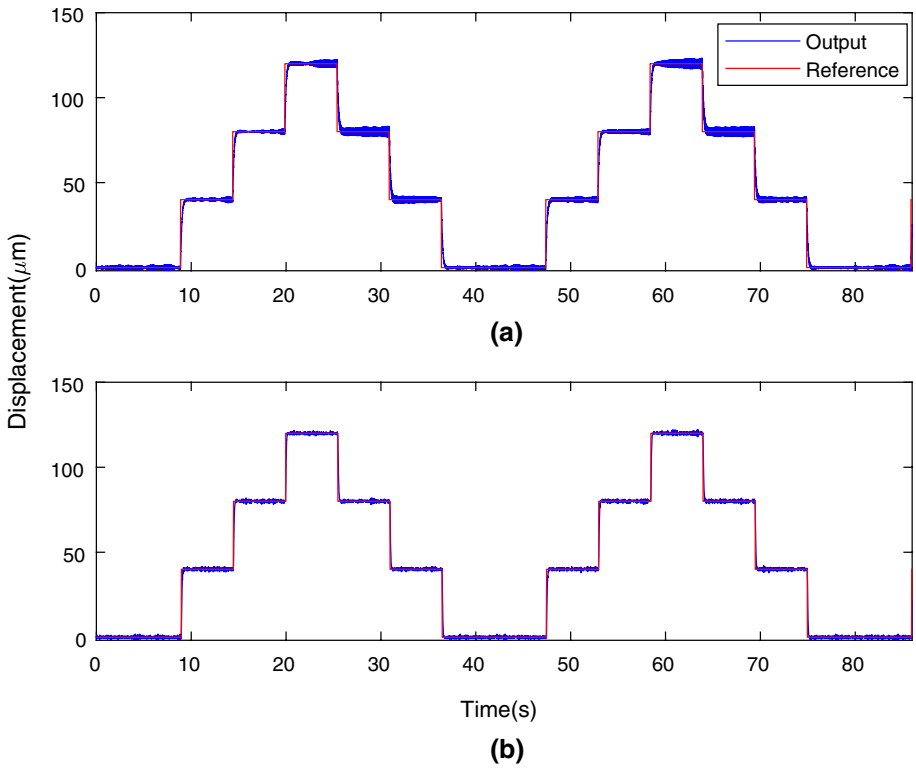

Fig. 16 Tracking performance under staircase reference. **a** Single stage, **b** Dual stage

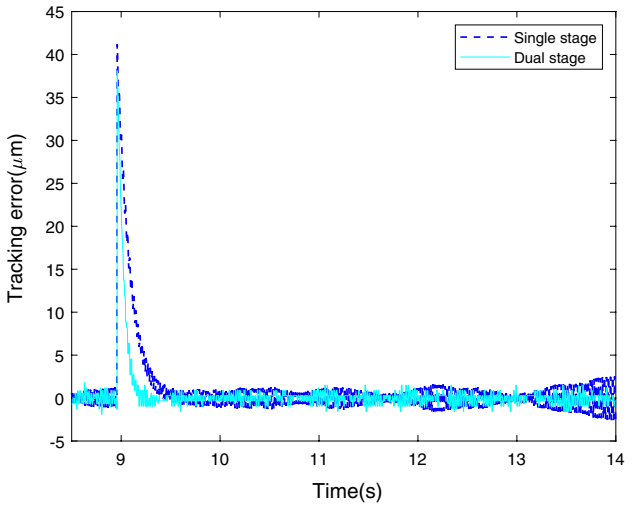

Fig. 17 Tracking error comparison between single stage and dual stage under the 40 μm staircase reference

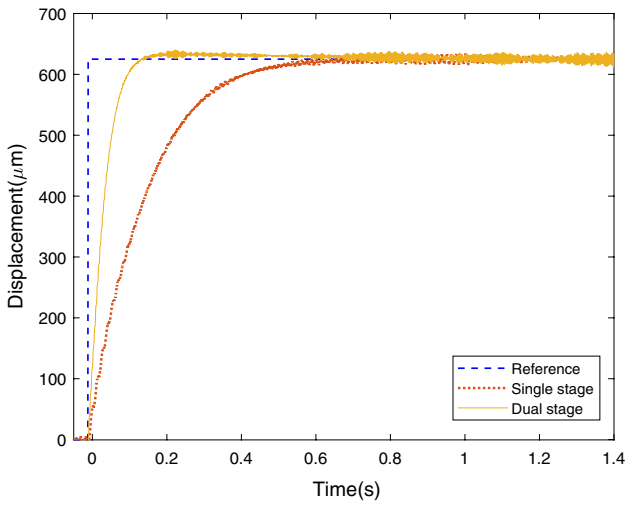

Fig. 18 Settling time comparison between single stage and dual stage under a 620 μm step reference

Lastly, the improvement of settling time was further verified with a larger 620-μm step response (i.e., the positioner's full motion range driven by the given piezoelectric actuator) as shown in Fig. 18. The results obtained from the experiments indicate a substantial discrepancy in settling time between the single stage and dual stage control systems. Specifically, the settling time for the single stage control was measured to be approximately 0.75 s. In contrast, the

Table 3 A comparison of FEM analysis and experimental results

Characteristics	Simulation	Experiment	Discrepancy (%)
First resonance frequency of dual-stage assembly (Hz)	80.47	77.71	−3.43
Displacement amplification ratio	29.57	28.17	−5
Max travel range (μm)	680	648	−4.71

dual stage control exhibited a significantly improved settling time of 0.25 s, showcasing an impressive 67% reduction in settling time. These findings underscore the substantial advantage of employing a dual stage control configuration in terms of achieving significantly faster and more efficient settling of the system's response.

Table 3 compares simulation data with actual experimental results, focusing on three main aspects, the first resonance frequency of a dual-stage assembly, the displacement amplification ratio, and the maximum travel range. According to the table, the first resonance frequency was simulated to be 80.47 Hz, but observed at 77.71 Hz, showing a slight discrepancy of −3.43%. The displacement amplification ratio was predicted to be 29.57 but measured at 28.17, leading to a −5% difference and the maximum travel distance was expected to be 680 μm and was actually μm, with a −4.71% variance. These differences are minor, suggesting that the simulation closely matches the experimental outcomes.

5 Conclusion

This paper presented the design, control and performance evaluation of a flexure-based micropositioner to achieve a longer travel range and higher precision by using the dual stage approach. It was shown that by using the bridge type mechanism a large amplification ratio of 28.17 was obtained to enlarge the travel range up to 648 μm and a second high-stiffness stage was designed to ensure the positioning accuracy of 1μm across the extended travel range. The improved performance was achieved under the dual stage control structure, which was also presented. The experimental results showed that the proposed dual stage micropositioner significantly reduced the tracking error and improved the disturbance rejection capability in comparison with the single stage positioner. These results demonstrate the effectiveness of the dual stage design in improving the overall performance of the system. Overall, this study provides important insights for the design and optimization of high-precision positioning systems for various applications.

Funding Open Access funding enabled and organized by CAUL and its Member Institutions

References

1. Salapaka, S., Sebastian, A., Cleveland, J. P., & Salapaka, M. V. (2002). High bandwidth nano-positioner: A robust control approach. *Review of Scientific Instruments, 73*(9), 3232–3241.
2. Kim, D., Kang, D., Shim, J., Song, I., & Gweon, D. (2005). Optimal design of a flexure hinge-based xyz atomic force microscopy scanner for minimizing abbe errors. *Review of Scientific Instruments, 76*(7), 073706.
3. Mohammad, T., & Salisbury, S. (2012). Design considerations for long travel z-axis ultra-precision positioning stage. *International Journal of Precision Engineering and Manufacturing, 13*, 1581–1588.
4. Lee, J., Seok, J.Y., Yang, M., & Kang, B. (2022). Facile fabrication of high-performance hybrid supercapacitor by one-step, self-grown copper nanopillar forest anchored with fe 3 o 4 anode. *International Journal of Precision Engineering and Manufacturing-Green Technology*, 1–11.
5. Binnig, G., & Rohrer, H. (2000). Scanning tunneling microscopy. *IBM Journal of research and development, 44*(1/2), 279.
6. Binnig, G., & Smith, D. P. (1986). Single-tube three-dimensional scanner for scanning tunneling microscopy. *Review of Scientific Instruments, 57*(8), 1688–1689.
7. Čeponis, A., & Mažeika, D. (2017). An inertial piezoelectric plate type rotary motor. *Sensors and Actuators A: Physical, 263*, 131–139.
8. Liu, Y., Yan, J., Xu, D., Chen, W., Yang, X., & Tian, X. (2016). An i-shape linear piezoelectric actuator using resonant type longitudinal vibration transducers. *Mechatronics, 40*, 87–95.
9. Cheng, T., He, M., Li, H., Lu, X., Zhao, H., & Gao, H. (2017). A novel trapezoid-type stick-slip piezoelectric linear actuator using right circular flexure hinge mechanism. *IEEE Transactions on Industrial Electronics, 64*(7), 5545–5552.
10. Liu, Y.-T. (2023). Recent development of piezoelectric fast tool servo (FTS) for precision machining. *International Journal of Precision Engineering and Manufacturing*, 1–24
11. Zhang, T., Tang, M., Li, H., Li, J., Zou, Y., Pan, Y., & Zhang, Z. (2022). A multidirectional pendulum kinetic energy harvester based on homopolar repulsion for low-power sensors in new energy driverless buses. *International Journal of Precision Engineering and Manufacturing-Green Technology, 9*(2), 603–618.
12. Cha, Y., & You, H. (2018). Torsion sensing based on patterned piezoelectric beams. *Smart Materials and Structures, 27*(3), 035010.
13. Lucinskis, R., Mazeika, D., & Bansevicius, R. (2018). Investigation of oscillations of piezoelectric actuators with multi-directional polarization. *Mechanical Systems and Signal Processing, 99*, 450–458.
14. Cheng, C.-H., & Hung, S.-K. (2015). A piezoelectric two-degree-of-freedom nanostepping motor with parallel design. *IEEE/ASME Transactions on Mechatronics, 21*(4), 2197–2199.
15. Lee, J., Dong, H., Ji, D.-Y., & Kundu, P. (2023). Cyber-physical systems framework for predictive metrology in semiconductor manufacturing process. *International Journal of Precision Engineering and Manufacturing Smart Technology, 1*, 107–113.
16. Sun, X., Chen, W., Zhang, J., Zhou, R., & Chen, W. (2015). A novel piezo-driven linear-rotary inchworm actuator. *Sensors and Actuators A: Physical, 224*, 78–86.
17. Ho, S.-T., & Jan, S.-J. (2016). A piezoelectric motor for precision positioning applications. *Precision Engineering, 43*, 285–293.
18. Lyu, Z., & Xu, Q. (2021). Recent design and development of piezoelectric-actuated compliant microgrippers: A review. *Sensors and Actuators A: Physical, 331*, 113002.

19. Iqbal, S., & Malik, A. (2019). A review on mems based micro displacement amplification mechanisms. *Sensors and Actuators A: Physical, 300*, 111666.
20. Qian, J., Yan, P., & Liu, P. (2021). Position/force modeling and analysis of a piezo-driven compliant micro-gripper considering the dynamic impacts of gripping objects. *Smart Materials and Structures, 30*(7), 075036.
21. Xing, Q., & Ge, Y. (2015). Parametric study of a novel asymmetric micro-gripper mechanism. *Journal of Advanced Mechanical Design, Systems, and Manufacturing, 9*(5), 0075–0075.
22. Wang, F., Shi, B., Tian, Y., Huo, Z., Zhao, X., & Zhang, D. (2019). Design of a novel dual-axis micromanipulator with an asymmetric compliant structure. *IEEE/ASME Transactions on Mechatronics, 24*(2), 656–665.
23. Gao, Q., Zhang, D., Xu, D., & Zhang, Z. (2012). A kinematics modeling and stress analysis method for flexible micro-gripper. In *2012 IEEE International Conference on Mechatronics and Automation*, pp. 825–830. IEEE
24. Wang, D., Yang, Q., & Dong, H. (2011). A monolithic compliant piezoelectric-driven microgripper: Design, modeling, and testing. *IEEE/ASmE Transactions on Mechatronics, 18*(1), 138–147.
25. Chen, F., Gao, Y., Dong, W., & Du, Z. (2020). Design and control of a passive compliant piezo-actuated micro-gripper with hybrid flexure hinges. *IEEE Transactions on Industrial Electronics, 68*(11), 11168–11177.
26. Wu, Z., & Xu, Q. (2018). Survey on recent designs of compliant micro-/nano-positioning stages. In *Actuators*, vol. 7, p. 5. MDPI
27. Lin, C., Shen, Z., Wu, Z., & Yu, J. (2018). Kinematic characteristic analysis of a micro-/nano positioning stage based on bridge-type amplifier. *Sensors and Actuators A: Physical, 271*, 230–242.
28. Ye, G., Li, W., Wang, Y.-q., Yang, X.-f., & Yu, L. (2010). Kinematics analysis of bridge-type micro-displacement mechanism based on flexure hinge. In *The 2010 IEEE International Conference on Information and Automation* (.–70). IEEE.
29. Xu, Q., & Li, Y. (2011). Analytical modeling, optimization and testing of a compound bridge-type compliant displacement amplifier. *Mechanism and Machine Theory, 46*(2), 183–200.
30. Xu, Q. (2013). New robust position and force regulation for a compliant microgripper. In *2013 IEEE International Conference on Automation Science and Engineering (CASE)* (pp. 801–806). IEEE
31. Lofroth, M., & Avci, E. (2019). Development of a novel modular compliant gripper for manipulation of micro objects. *Micromachines, 10*(5), 313.
32. Das, T. K., Shirinzadeh, B., Al-Jodah, A., Ghafarian, M., & Pinskier, J. (2021). A novel compliant piezoelectric actuated symmetric microgripper for the parasitic motion compensation. *Mechanism and Machine Theory, 155*, 104069.
33. Lee, J., Chua, P. C., Chen, L., Ng, P. H. N., Kim, Y., Wu, Q., Jeon, S., Jung, J., Chang, S., & Moon, S. K. (2023). Key enabling technologies for smart factory in automotive industry: Status and applications. *International Journal of Precision Engineering and Manufacturing, 1*(1), 94–105.
34. Chen, X., & Li, Y. (2021). A new structure to achieve large-scale damage-avoiding capture based on compliant mechanism. *Microsystem Technologies, 27*, 937–944.
35. Chen, X., Deng, Z., Hu, S., Gao, J., & Gao, X. (2020). Designing a novel model of 2-DoF large displacement with a stepwise piezoelectric-actuated microgripper. *Microsystem Technologies, 26*, 2809–2816.
36. Yang, Y.-L., Wei, Y.-D., Lou, J.-Q., Xie, F.-R., & Fu, L. (2015). Development and precision position/force control of a new flexure-based microgripper. *Journal of Micromechanics and Microengineering, 26*(1), 015005.
37. Zhang, D., Zhang, Z., Gao, Q., Xu, D., & Liu, S. (2015). Development of a monolithic compliant SPCA-driven micro-gripper. *Mechatronics, 25*, 37–43.
38. Wang, F., Liang, C., Tian, Y., Zhao, X., & Zhang, D. (2014). Design of a piezoelectric-actuated microgripper with a three-stage flexure-based amplification. *IEEE/ASME Transactions on Mechatronics, 20*(5), 2205–2213.
39. Lu, K., Zhang, J., Chen, W., Jiang, J., & Chen, W. (2014). A monolithic microgripper with high efficiency and high accuracy for optical fiber assembly. In *2014 9th IEEE Conference on Industrial Electronics and Applications* (pp. 1942–1947). IEEE.
40. Carrozza, M. C., Eisinberg, A., Menciassi, A., Campolo, D., Micera, S., & Dario, P. (2000). Towards a force-controlled microgripper for assembling biomedical microdevices. *Journal of Micromechanics and Microengineering, 10*(2), 271.
41. Liang, C., Wang, F., Shi, B., Huo, Z., Zhou, K., Tian, Y., & Zhang, D. (2018). Design and control of a novel asymmetrical piezoelectric actuated microgripper for micromanipulation. *Sensors and Actuators A: Physical, 269*, 227–237.
42. Liang, C., Wang, F., Tian, Y., Zhao, X., & Zhang, D. (2017). Development of a high speed and precision wire clamp with both position and force regulations. *Robotics and Computer-Integrated Manufacturing, 44*, 208–217.
43. Wu, Z., & Li, Y. (2021). Design and control of a novel microgripper using adaptive backstepping slide mode control method. *Microsystem Technologies*, 1–13
44. Zhang, M., Cui, X., Xiu, Q., Zhuang, J., & Yang, X. (2023). Dynamic modeling and controlling of piezoelectric actuator using a modified Preisach operator based Hammerstein model. *International Journal of Precision Engineering and Manufacturing, 24*(4), 537–546.
45. Chen, X., Zhang, S., Bao, X., & Zhao, H. (2008). Master and slave control of a dual-stage for precision positioning. In *2008 3rd IEEE International Conference on Nano/Micro Engineered and Molecular Systems* (pp. 583–587). IEEE.
46. Lee, S.-H., Kim, Y.-H., & Chung, C. C. (2001). Dual-stage actuator disk drives for improved servo performance: Track follow, track seek, and settle. *IEEE Transactions on Magnetics, 37*(4), 1887–1890.
47. Young, P.M., Morris, J.C., & Ho, H.T. (2003). Servo control of a dual-stage actuator for a high performance disk drive. part 2: controller design and implementation. In *Proceedings of the 2003 American Control Conference, 2003* (vol. 3, pp. 2529–2534). IEEE.
48. Chung, C. C., Seo, C. W., & Lee, S.-H. (2000). Two degree-of-freedom dual-stage actuator controller design for hard disk drives. *IEEE Transactions on Magnetics, 36*(5), 2255–2257.
49. Yong, Y. K., & Lu, T.-F. (2008). The effect of the accuracies of flexure hinge equations on the output compliances of planar micro-motion stages. *Mechanism and Machine Theory, 43*(3), 347–363.
50. Chen, G., & Howell, L. L. (2009). Two general solutions of torsional compliance for variable rectangular cross-section hinges in compliant mechanisms. *Precision Engineering, 33*(3), 268–274.
51. Ueda, J., Secord, T. W., & Asada, H. H. (2009). Large effective-strain piezoelectric actuators using nested cellular architecture with exponential strain amplification mechanisms. *IEEE/ASME Transactions on Mechatronics, 15*(5), 770–782.
52. Choi, K.-B., Lee, J. J., Kim, G. H., Lim, H. J., & Kwon, S. G. (2018). Amplification ratio analysis of a bridge-type mechanical amplification mechanism based on a fully compliant model. *Mechanism and Machine Theory, 121*, 355–372.
53. Das, T. K., Shirinzadeh, B., Ghafarian, M., & Al-Jodah, A. (2020). Design, analysis, and experimental investigation of a single-stage and low parasitic motion piezoelectric actuated microgripper. *Smart Materials and Structures, 29*(4), 045028.
54. Mohd Zubir, M. N., Shirinzadeh, B., & Tian, Y. (2009). Development of novel hybrid flexure-based microgrippers for precision

micro-object manipulation. *Review of Scientific Instruments, 80*(6), 065106.
55. Chen, W., Qu, J., Chen, W., & Zhang, J. (2017). A compliant dual-axis gripper with integrated position and force sensing. *Mechatronics, 47*, 105–115.
56. Ekbatani, R.Z., Zheng, J., Chen, X., Nikzad, M., & Man, Z. (2023). A novel compact compliant bridge type micro-positioning stage with a large displacement amplification ratio. In *2023 International Conference on Advanced Mechatronic Systems (ICAMechS)* (pp. 1–6). IEEE
57. Kindt, J. H., Fantner, G. E., Cutroni, J. A., & Hansma, P. K. (2004). Rigid design of fast scanning probe microscopes using finite element analysis. *Ultramicroscopy, 100*(3–4), 259–265.

Romina Zarrabi Ekbatani graduated with a Bachelor's degree in Mechanical Engineering from the University of Tehran in 2018. In 2020, she advanced her academic career by becoming a PhD student and tutor at Swinburne University. Initially concentrating on soft robotics, Romina's research focus has since shifted towards piezoelectric actuators, dual-stage control, and reinforcement learning, fields in which she is actively contributing.

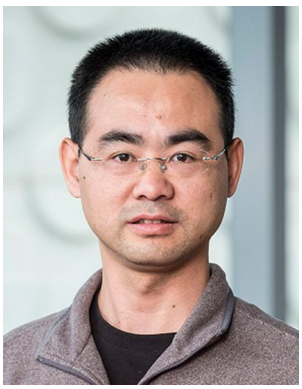

Prof Jinchuan Zheng received the B.Eng. and M.Eng. degrees in mechatronics engineering from Shanghai Jiao Tong University, Shanghai, China, in 1999 and 2002, respectively, and the Ph.D. degree in electrical and electronic engineering from Nanyang Technological University, Singapore, in 2006. In 2005, he joined the Australian Research Council (ARC) Centre of Excellence for Complex Dynamic Systems and Control, School of Electrical and Computer Engineering, the University of Newcastle, Callaghan, NSW, Australia, as a Research Academic. From 2011 to 2012, he was a Staff Engineer with the Western Digital Hard Disk Drive R&D Center, Singapore. Since 2012, he has been with Swinburne University of Technology, Melbourne, VIC, Australia. He is currently a Professor with the School of Science, Computing and Engineering Technologies. His research interests include high precision motion control systems, electric vehicle control technology, mobile robots, and biomechatronic devices.

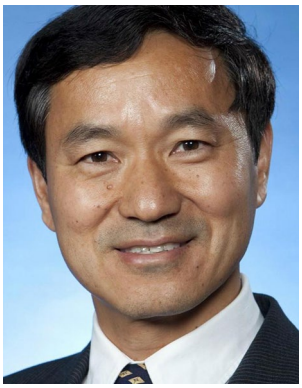

Prof XiaoQi Chen Ph.D. (Liverpool, 1989), is the Dean at the Shien-Ming Wu School of Intelligent Engineering, South China University of Technology (SCUT). Prior to joining SCUT, he was Deputy Director of Manufacturing Futures Research Institute, Swinburne University of Technology till 2022; Professor, Director of Mechatronics Engineering, University of Canterbury (2006-2019); Senior Scientist and Technical Manager, Singapore Institute of Manufacturing Technology (1992-2006). His research focuses on robotics, advanced materials processing, industrial IOT and autonomous systems. His team received Singapore National Technology Award (1999) for their work on robotic system for re-manufacturing aeroengine components. He was awarded New Zealand Forest Owners Association Award (2015) for the development of forest harvest robot. His novel work on untethered wall climbing robot span off Invert Robotics Ltd that won New Zealand Hi-Tech Start-Up Excellence Award (2012). He has over 400 publications, 10 patents, 4 books; and has delivered over 100 keynote speeches. He has been elected to F.RSNZ, F.EngNZ, F.SME and F.ASME.

Dr. Mostafa Nikzad is a mechanical engineer with specialisation in composite materials, modelling and advanced manufacturing. With a Master of Science majoring in electro-physical deposition processes, and a PhD in additive manufacturing of metal/polymer composites, his research focuses on the interdisciplinary areas of applied material science and advanced manufacturing. As a researcher he has over 14 years' experience in design and development of composite materials with pioneering work on 3D printing of composites in collaboration with CSIRO and international research organisations as well as working with multitude of industrial giants such as Fuchs LUBRITECH, CITROEN Messian Durand, Tesla, Ford, Henkel and various others overseas and in Australia. Currently he is a senior lecturer in Mechanical and Product Design Engineering with a passion for translational science and industry-focused research and development activities.

Prof Zhihong Man earned his B.Eng from Shanghai Jiaotong University, China (1982), M.Sc from Chinese Academy of Sciences (1987), and PhD from the University of Melbourne, Australia (1994). He served as a Lecturer and Senior Lecturer at Edith Cowan University, Perth (1994-1996), and the University of Tasmania (1996-2001). In 2001, he was a Visiting Senior Fellow at Nanyang Technological University (NTU), Singapore, later becoming Associate Professor of Computer Engineering (2002-2007). From 2007 to 2008, he worked at Monash University Sunway Campus, Malaysia, as a Professor and department head. He is now a Professor of Robotics and Mechatronics at Swinburne University of Technology, Melbourne. Zhihong's research spans nonlinear control, signal processing, robotics, and more, resulting in over 200 publications. He has held editorial and chair roles in numerous international conferences and received accolades including the Nanyang Technological University Best Teacher Award (2004) and Most Popular Lecturer at NTU's School of Computer Engineering (2002-2007).